Math. Model. Nat. Phenom. 19 (2024) 16
https://doi.org/10.1051/mmnp/2024013

Mathematical Modelling of Natural Phenomena
www.mmnp-journal.org

PATIENT-SPECIFIC INPUT DATA FOR PREDICTIVE MODELLING OF THE FONTAN PROCEDURE

Tatiana Dobroserdova[1,*], Lyudmila Yurpolskaya[2], Yuri Vassilevski[1,3] and Andrey Svobodov[4]

Abstract. Personalized blood flow models are used for optimization of the Fontan procedure. In this paper we discuss clinical data for model initialization. Before the Fontan procedure patients undergo CT or MRI examination. Computational domain of interest is reconstructed from this data. CT images are shown to have a better spatial resolution and quality and are more suitable for segmentation. MRI data gives information about blood flow rates and it is utilized for setting boundary conditions in local 3D hemodynamic models. We discovered that the MRI data is contradictory and too inaccurate for setting boundary conditions: the error of measured velocities is comparable with blood velocities in veins. We discuss a multiscale 1D3D circulation model as potentially suitable for prediction of the Fontan procedure results. Such model may be initialized with more reliable data (MR measurements of blood flow in aorta and ultrasound examination of easily accessible vessels) and take into account collateral and fenestration blood flows which are typical for Fontan patients. We have calculated these flow rates for several patients and demonstrated that such flows occur systematically.

Mathematics Subject Classification. 76-10, 65Z05.

Received December 11 2023. Accepted June 7, 2024.

1. Introduction

Single ventricle pathology includes the set of rare and complex anomalies with the presence of either single anatomical or single functional ventricle. Multistage hemodynamic correction, which contributes to gradual adaptation of the cardiovascular system, is prescribed for patients with congenital heart defects (CHD). Conventionally, the first stage is the formation of a systemic-pulmonary shunt in the birth period in order to prepare the pulmonary bed for subsequent operations. At the second stage the bidirectional cavapulmonary anastomosis BCPA is constructed (the Glen operation), when the pulmonary trunk is separated from the heart and the superior vena cava is sutured to the pulmonary artery. The final stage is formation of the total cavapulmonary

Keywords and phrases: Mathematical modelling, Fontan procedure, segmentation, congenital heart defects, MRI, CT.

[1] Marchuk Institute of Numerical Mathematics of the Russian Academy of Sciences, 8 Gubkina str., Moscow 119333, Russia.
[2] A. N. Bakulev National Medical Research Center of Cardiovascular Surgery of the Ministry of Health of the Russian Federation, Rublevskoe Shosse 135, Moscow 121552, Russia.
[3] Moscow Institute of Physics and Technology (National Research University), 9 Institutskiy per., Dolgoprudny, Moscow Region 141701, Russia; Sechenov University, 8-2 Trubetskaya str., Moscow 119991, Russia; Sirius University, Olympic pr., 1, Sochi 354340, Russia.
[4] State Budgetary Healthcare Institution of Moscow Region Children's Clinical Hospital named after L.M.Roshal, 85 Varshavskoe Shosse, derevnia Borodino, Podolsk, Moscow Region 142117, Russia.

* Corresponding author: DobroserdovaTK@gmail.com

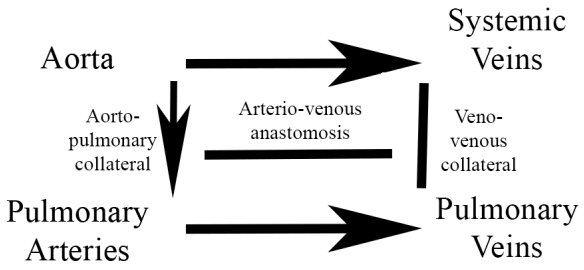

FIGURE 1. Scheme of collateral blood flow in a patient with single ventricle.

connection TCPC (the Fontan procedure) which redirects blood from the inferior vena cava to the pulmonary arteries.

The Fontan procedure has been modified significantly since its introduction in 1971, in order to improve treatment results. The class of patients suitable for surgery has become wider. The choice of surgical correction method and time of procedure, balance of the resulted blood flow distribution from vena cava to pulmonary arteries affect the quality and expectancy of life [1, 2]. Patients with Fontan circulation suffer from many inevitable complications [3], likely due to increased systemic venous pressure [4, 5]. It remains unclear why decompensation happens for some of them and others do not have any specific symptoms. Due to this reason, all patients undergoing Fontan surgery require careful clinical monitoring using imaging techniques.

Model-based understanding of the Fontan circulation and optimization of the Fontan procedure for real patients gives a chance to improve the prognosis. 3D blood flow models allow clinicians to test different vessel configurations to minimize pulmonary and TCPC resistance, energy dissipation in TCPC, to balance the hepatic and the whole flow distribution between the right and left lungs and avoid regions with too high or too low wall shear stress [6, 7].

Local 3D blood flow modelling is a common choice for the solution of such problem [6–8]. The model is based on the Navier–Stokes equations. The domain of interest consists of vena cava and pulmonary arteries. The preoperative 3D vascular geometry is reconstructed from computed tomography (CT) or magnetic resonance imaging (MRI) data. Mean values or pulsatile waveforms of flow rates derived from phase contrast MRI are usually prescribed as inflow and sometimes as outflow patient-specific boundary conditions. Resistance and Windkessel-type outflow boundary conditions are used to represent flow distribution between pulmonary arteries and values of catheterization pressure if available. Impedance outflow boundary conditions may take into account patient-specific anatomy of downstream pulmonary vascular tree and adjust measured pressure. Local models cannot take into account significant changes of boundary conditions in postoperative period [9] and this is the crucial disadvantage of such models for surgery outcome prediction.

Models of blood circulation avoid this issue and provide postoperative boundary conditions in the domain of interest. Moreover, they can take into account pathologies and predict possible complications outside the domain of interest. One more important advantage of circulation models is their ability to take into account collateral and fenestration blood flows which are features of the Fontan circulation. Collateral blood flow may occur at different levels of circulation (Fig. 1). Most of aortopulmonary collaterals are closed in the early childhood. Veno-venous communications become the main source of severe shunting and may contribute to excessive volume loading of the systemic ventricle [10]. Fenestrations are created to increase cardiac output. Fenestration flow from the conduit to the right atrium in the immediate postoperative period could be as much as 30–40% of the cardiac output and decreases in a distant period. Low fenestration flow may be associated with decreased diastolic function [11].

Closed-loop multiscale 0D-3D model was developed in [9] for a patient with the Fontan circulation: a lumped parameter model of the whole cardiovascular system was coupled with a 3D local blood flow model in a patient-specific domain of BCPA or TCPC and pulmonary arteries. In our previous work [12] we constructed a patient-specific 1D-3D multiscale model of the Fontan circulation: systemic part was represented by a 1D model and

TCPC was represented by the 3D model. Developing of full circulation model demands more patient-specific data to construct the vascular network and to tune the flow. At the same time 1D part of multiscale model can be initialized based on available and reliable ultrasound data [13].

Before the Fontan procedure, patients with BCPA undergo ultrasound examination of blood vessels. Ultrasound examination is a cheap and accessible first-line method of diagnostics, which is used for routine monitoring. These blood velocity measurements are not suitable for setting boundary conditions directly without knowing the velocity profile in the vascular cross-section. Eccentric blood flow, lying outside the scanning plane, could be hardly estimated by echocardiography. Moreover, this method has visibility limitations for deep vessels such as superior vena cava (SVC), inferior vena cava (IVC), left pulmonary artery (LPA) and right pulmonary artery (RPA) and limitations for blood velocity measurements in them [14–16].

Catheterization and ultrasound examination may be used for estimation of the pressure gradient and blood flow in fenestration. The average pressure gradient in the fenestration corresponds to the transpulmonary gradient in the absence of stenoses and should be equal to 5–8 mmHg [17]. Catheterization is prescribed for the measurement of certain hemodynamic parameters and only for those patients who are expected to undergo intervention during the same procedure. The resulted measurements may be inaccurate for setting boundary conditions since the solution of hydrodynamic problem is very sensitive to the prescribed pressure drop.

CT and MRI methods play a key role in diagnostics [17–19]. CT is preferred due to high contrast, spatial resolution and less interference from metal implants such as stents. This examination is prescribed for most patients before and after the Fontan procedure in order to provide 3D geometry of all anatomical structures in the scan region. However, CT scanning does not provide any information about blood flows. Ultrasound and CT examinations are assigned for most patients and considered to be sufficient for surgery planning.

For some patients it is difficult to perform the ultrasound examination because of anatomical features. For others, results of dopplerography do not correspond to anamnesis. In such cases MRI is prescribed to understand the necessity of the Fontan procedure.

In this paper we discuss clinical data which is gathered under standard medical examinations and may be used for patient-specific model initialization.

2. Reconstruction of 3D computational domain

2.1. Medical examinations: CT vs MRI

CT and MRI are two types of medical examinations which provide 3D geometry of the heart and main vessels. Obtaining high-quality images of the domain of interest is challenging because of hemodynamic and anatomical features of patients with CHD, especially children. Depending on the clinical picture, they are assigned either CT or MRI. Discussions about the choice of CT or MRI for such patients are still ongoing [20, 21]. For some CHD MRI has the high 1 diagnostic level of evidence. MRI is better than CT in time resolution: 20–50 ms for MRI and 50–135 ms for CT [21, 22]. At the same time the spatial resolution of CT is provided by an isotropic voxel of size 0.5 mm. MRI loses to CT in the spatial resolution: minimal voxel size is 0.8 mm, and it is not yet isotropic in standard scans. The clarity of the MR image is inferior to CT (*cf.* Fig. 2), the sensitivity of the method decreased significantly in vessels with small diameters and/or low blood velocity. MRI scanner software provides high-resolution series of a small domain of interest, but not for the whole heart because of scanning duration.

CT with intravenous contrast is prescribed in most cases of routinely performed medical examinations before and after Fontan procedure because of better spatial resolution, the speed of scanning (procedure takes 5–10 min), applicability for patients in critical condition, one-time assessment of the lung parenchyma. Moreover, it is possible to obtain simultaneously information about the liver without increasing the time of the CT at the cost of higher radiation dose. The quality of CT images may deteriorate: for heart rate exceeding 80 beats per minute, for patients with heart failure and arrhythmia incapable to hold breath, having reduced blood flow in the conduit and consequent poor contrast in it, difficulties in selecting the contrast phase. CT examination does not provide quantitative information about hemodynamics and creates a radiation load on the body.

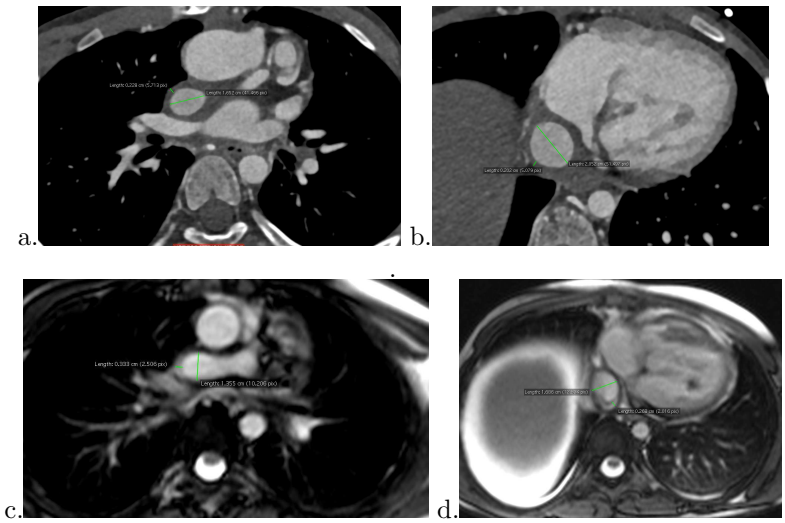

FIGURE 2. Comparison of CT (a, b) and MR (c, d) scans in the transverse plane of a patient with Fontan circulation. Levels of connection of conduit and SVC (a, c) or IVC (b, d).

MRI is prescribed less frequently than CT, in order to match specific purposes: to calculate functional parameters of the heart and blood flow characteristics, 4D flow mapping to assess the vascular geometry and blood flow distribution, search for fibrotic changes in the myocardium with conduit assessment *via* 3D angiography. MRI scanning the heart and blood vessels takes about 40 min. Younger patients require deep sedation and therefore duration of scan should be minimal. MRI of the liver is performed as an additional study, the time of the procedure becomes significantly longer. State of patients after the Fontan procedure often does not permit the use of MRI, only CT angiography is performed in order to assess the conduit, chest organs, and liver. MRI for patients with stents or clips on the vessels is unacceptable as they distort real parameters of blood flow. The quality of MR images may be also reduced because of artefacts due to heart rhythm disorder and signs of heart failure (fluid in cavities, dyspnea).

2.2. Method of image segmentation

In this paper, a semi-automated algorithm is used to segment the heart and main vessels. The algorithm works both with CT and MRI data. It is based on the snake evolution method [23]. The snake is a closed surface which is manually initialized with one or several spherical bubbles in the domain of interest. Further, this bubble automatically expands and possibly merges until the snake approximates the segmentable organ. The growth of the snake follows the velocity of each point of the snake boundary at each time moment. The velocity vector is orthogonal to the surface and depends on its curvature at a given point, edges of the input image and local homogeneity of the intensity. The algorithm is applied in the ITK-SNAP software package [23].

Predictive numerical modelling of the Fontan procedure requires a computational mesh in the domain of interest composed of vena cava and pulmonary arteries. Additionally, a mesh of heart chambers may be required for modelling of fenestrations or surgical techniques without extracardiac conduit. Since meshing and numerical simulation are out of the scope of this paper, we do not address their details [13].

2.3. CT-based reconstruction of the domain of interest for patients with CHD

We present segmentations of heart chambers and vessels for CT data of 4 anonimized patients listed in Table 1. The examinations were carried out on the SOMATOM Definition Flash CT scanner with the volumetric scanning program with minimal slice thickness 0.6 mm, ECG synchronization and intravenous bolus contrast

TABLE 1. Information about patients.

Patient	Age	Status
A	17	CHD, Fontan circulation
B	18	CHD, Fontan circulation
C	6	CHD, BCPA
D	7	CHD, BCPA

1	Aorta	9	RPA	16	Single atrium
2	SVC	10	Pulmonary trunk	17	Coronary sinus
3	Conduit	11	Right ventricle	18	Right coronary artery
4	Asygos vein	12	Left ventricle	19	Left coronary artery
5	IVC	13	Single ventricle	20	Pulmonary arteries
6	LPV	14	Right atrium	21	Pulmonary veins
7	LPA	15	Left atrium	22	Coronary arteries
8	RPV				

FIGURE 3. Legend of colors in segmentation from Figures 4–8.

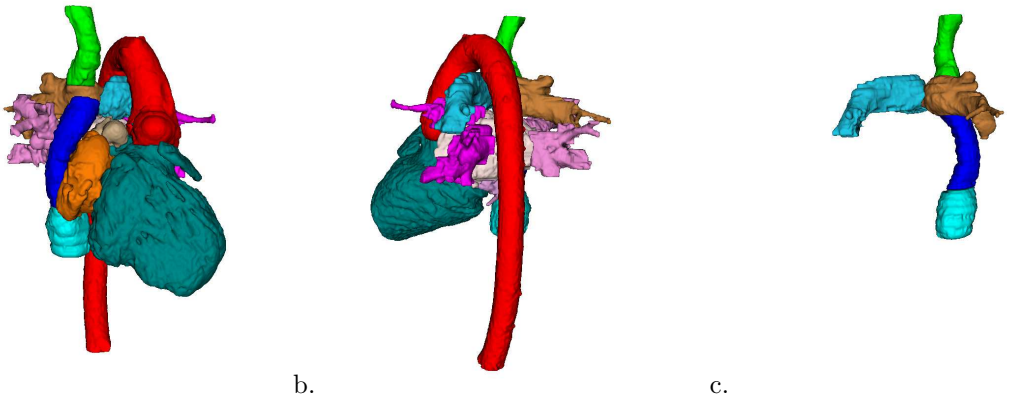

a. b. c.

FIGURE 4. Patient A. Segmentation: (a) front view; (b) back view; (c) TCPC.

agent “Omnipack-350”. Data acquisition was performed according to the standard study protocol. Four selected patients with CHD have different age and status: two of them with the Fontan circulation, two of them have BCPA. The legend of colors is presented in Figure 3. The resulted segmentations are presented in Figures 4–8: (a) front view; (b) back view; (c) vena cava and pulmonary arteries. Segmentation results were evaluated by a radiologist and are anatomically correct. Reconstructed domains are suitable for further predictive numerical modelling.

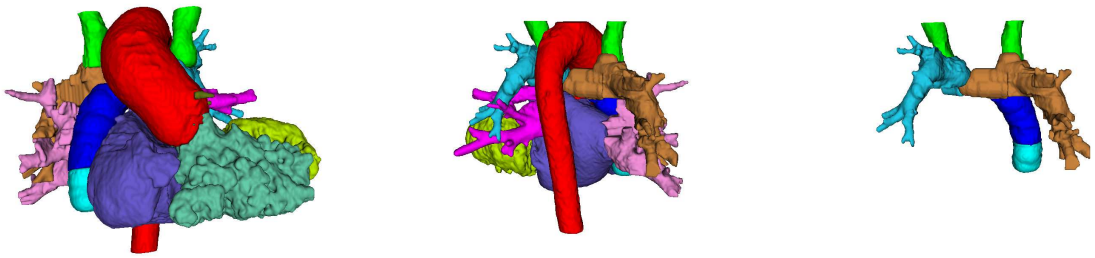

a. b. c.

FIGURE 5. Patient B. Segmentation: (a) front view; (b) back view; (c) TCPC.

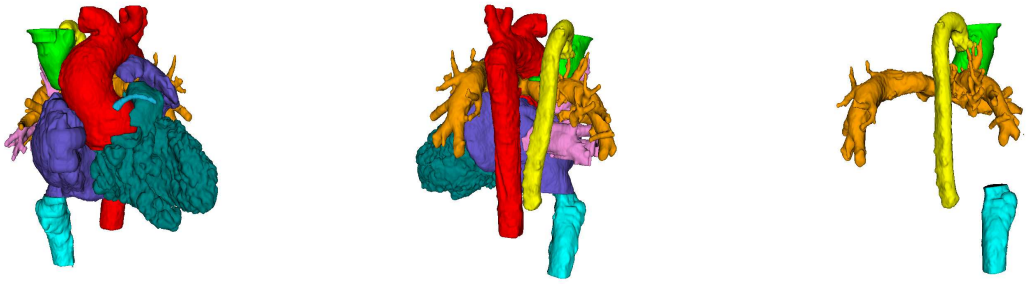

a. b. c.

FIGURE 6. Patient C. Segmentation: (a) front view; (b) back view; (c) BCPA.

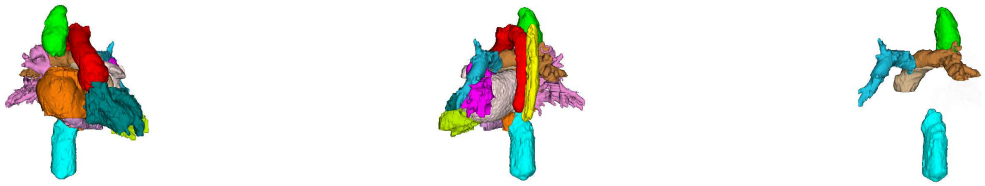

a. b. c.

FIGURE 7. Patient D. Segmentation: (a) front view; (b) back view; (c) BCPA.

2.4. Comparison of segmentations of CT and MRI data

We compared the segmentation algorithm for CT and MRI data of the same female patient E. CT examination (see above) was performed at the age 22 months when BCPA was formed. MR examination was performed at the age 4 years after the Fontan procedure with implanted conduit. The examination was performed according to the standard protocol on a Siemens 1.5 Tesla Avanto MR tomograph, using a multichannel surface coil for scanning, ECG synchronization. The slice thickness was 5–7 mm. The results of segmentation are shown in Figure 8 for CT (a–c) and MRI (d–f).

The segmented domain based on the MRI data is significantly smaller than the same domain for the same patient based on the CT data although the patient becomes older. Pulmonary veins are not visualized on MRI scans. The section of the aorta is not seen precisely and is reconstructed based on operator's experience.

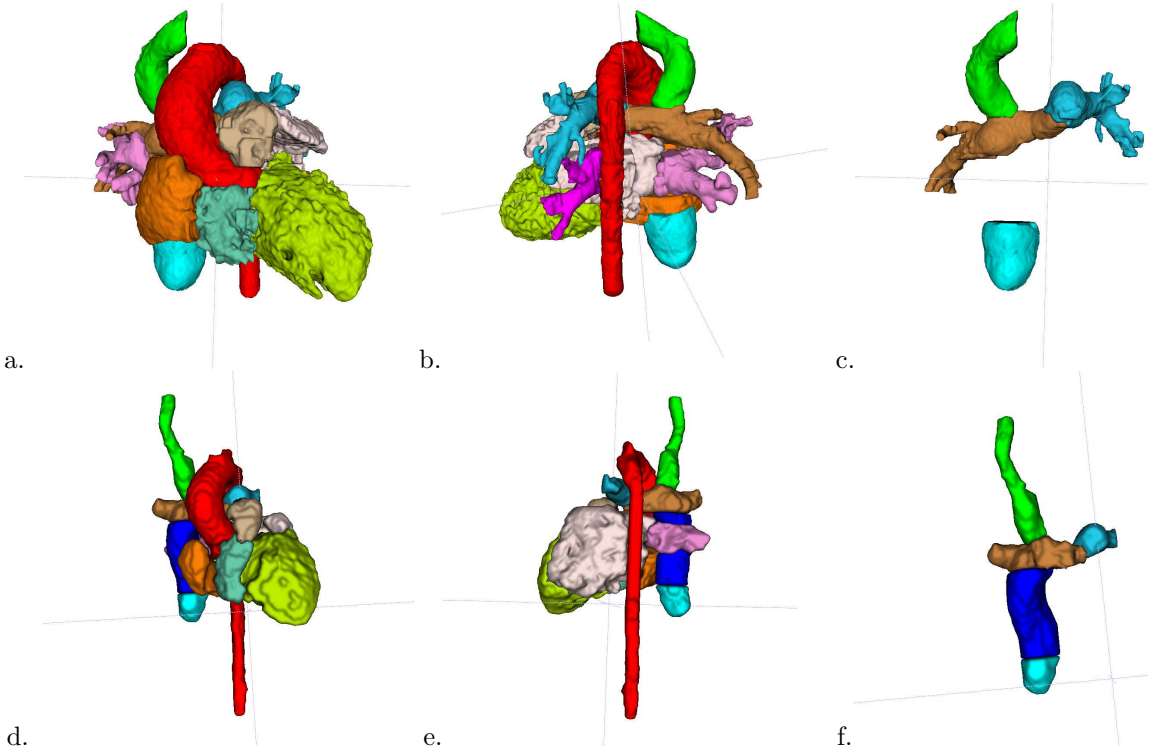

FIGURE 8. Patient E. Comparison of CT (a–c) and MR (d–f) segmentations: (a, d) front view; (b, e)back view; (c, f)the domain of interest.

3. Boundary conditions for flow in cavapulmonary anastomosis

3.1. 4D flow MRI

4D flow MRI (or time-resolved 3D flow magnetic resonance imaging) is the main tool for quantitative assessment of blood flow in patients with CHD. It provides blood flow rates and velocities, as well as areas of vascular cross-sections. For diagnostics the following vessels of interest are examined: ascending aorta (Ao), IVC, SVC, LPA, RPA and left and right pulmonary veins (LPV and RPV).

Velocity encoding (VENC) is a parameter of MRI scanning which is specified before the procedure. The VENC value should exceed the highest value of blood velocity in the vessel of interest to provide the correct flow assessment. If the selected VENC is set too high, quality of the data deteriorates: vessels with slow flow will not be visible or measurements in them will be noisy, small blood velocity differences will not be distinguishable. If the selected VENC is set too low, faster flows will not be appropriately represented [24, 25].

During 4D flow MRI mapping VENC is set conventionally to 80–100 $\mathrm{cm\,s^{-1}}$, less often to 150 $\mathrm{cm\,s^{-1}}$ for both aortic and venous blood flow. This is a compromise between reduction of examination time and simultaneous acquisition of flow data at different vessels including small venous vessels. With such VENC, flow rate in aorta may be underestimated and flow rate in veins and pulmonary arteries may be represented inaccurately.

The results of MR 4D flow mapping depend significantly on the VENC setting, noise, low spatial resolution, segmentation during post-processing, presence of eddy currents [26–29]. The cumulative error rate may achieve 22.5% [28]. Quantitative results based on free-breathing MRI data may also be affected by the difference between respiratory cycles because vena cava carries blood to the pulmonary arteries [30].

In our previous research we showed that flow rates measured by 4D flow MRI should be used as boundary conditions in mathematical models with great caution [12]. After the Fontan procedure, aortic flow rate should

TABLE 2. 4D flow MRI measurements of net forward volume [ml] for 25 Fontan patients in Aorta (Ao) and Vena Cava (VC), Pulmonary arteries and veins (PA and PV): inferior and Superior Vena Cava (IVC and SVC), conduit (cond), Right and Left pulmonary arteries (RPA and LPA) and veins (RPV and LPV).

No	Age	Ao	IVC	SVC	cond	RPA	LPA	LPV	RPV	VC	PA	PV
1	12	30	9	8	6	5	14			17	19	
2	28	78,5	37	17	31	33	32			54	65	
3	20	48	23	6	25	19	18			29	37	
4	33	72	53	17	52	35	25			70	60	
5	5	23	10	8	10	9	7			18	16	
6	35	74	61	8,5		6	2			69,5	8	
7	3	21	10	11	11	15	7			21	22	
8	52	77	25	10		15	4			35	19	
9	27	58	33	17	56	46	15			50	61	
10	5	24,5	10	7,5	10	8,5	7,5			17,5	16	
11	21	26	15	12	9	8	25			27	33	
12	34	49	21	5	23	14	24			26	38	
13	35	181	63	27		28	88			90	116	
14	16	37	17	4	9	5.4	7.8			21	13.2	
15	22	77	37	17	42	11	19			54	30	
16	17	49	13	14	11	15	15			27	30	
17	14	29.5	11.3	9.2	8.9	10.9	9.8			20.5	20.7	
18	12	36	8.3	8.6		5.6	13.3	6.5	9.8	16.9	18.9	16.3
19	11	42	20	17		14	14	14.4	17.9	37	28	32.3
20	6	23	14	12		2	9	11	8	26	11	19
21	13	53	24	11		16	5	6.5	16.5	35	21	23
22	13	25	7	7		36	4	4.1	25.7	14	40	29.8
23	11	18	12	9		7	9	5.7	5.2	21	16	10.9
24	12	25	12	6		6	7	18.6	13	18	13	31.6
25	12	23	12	5		4	3	9	9.1	17	7	18.1

be equal to the total systemic venous return (the sum of the flow rates in IVC and SVC) and the pulmonary arterial flow (the sum of the flow rates in the LPA and RPA), as well as the total pulmonary venous return (the sum of the flows in the LPV and RPV). In practice, however, measurements violate these equalities. Measurement errors, presence of regurgitation, fenestration, or significant systemic collateral blood flow are known to be possible reasons for such discrepancy [31].

3.2. Critical analysis of 4D flow MRI data

Construction of patient-specific blood flow models presumes their calibration to reproduce patient's time flow rate profiles. Flow rates are more preferred as data for model calibration than blood velocities as the flow rates do not depend on the unknown velocity profiles in vascular cross-section. In this paper we analyze net forward blood volume during one cardiac cycle measured by 4D flow MRI tool. The average net flow rate is equal to the net forward volume divided by duration of the cardiac cycle.

We analyzed 4D flow MRI data of 25 Fontan patients shown in Table 2. The examination was performed in A.N. Bakulev National Medical Research Center for Cardiovascular Surgery on Siemens 1.5 Tesla Avanto MR tomograph. Measurements are presented on levels of ascending aorta, SVC, IVC, conduit, LPA, RPA. For 8 patients with the Fontan circulation without clinical signs of decompensation (patients 18–25) the net forward blood volume in LPV and RPV was calculated. The total volumes in vena cava ($V_{VC} = V_{IVC} + V_{SVC}$), pulmonary arteries ($V_{PA} = V_{LPA} + V_{RPA}$) and pulmonary veins($V_{PV} = V_{LPV} + V_{RPV}$) are shown in the last

TABLE 3. Net forward blood volume in Vena Cava, Pulmonary arteries and veins (VC, PA, PV) – Cols. 2–4; returning through the veins (VR) – Col. 5; in fenestration – Cols. 6–7; in collaterals – Cols. 8–9 relative to the net forward volume in Aorta (Ao) for Fontan patients calculated based on 4D flow MRI measurements.

1	2	3	4	5	6	7	8	9
No	$\frac{V_{VC}}{V_{Ao}}$	$\frac{V_{PA}}{V_{Ao}}$	$\frac{V_{PV}}{V_{Ao}}$	$\frac{V_{VR}}{V_{Ao}}$	$\frac{V_{IVC}-V_{cond}}{V_{Ao}}$	$\frac{V_{VC}-V_{PA}}{V_{Ao}}$	$\frac{V_{SC}}{V_{Ao}}$	$\frac{V_{PC}}{V_{Ao}}$
1	0.57	0.64			0.10	–0.07	0.43	
2	0.69	0.83			0.08	–0.14	0.31	
3	0.61	0.78			–0.04	–0.17	0.40	
4	0.98	0.84			0.01	0.14	0.03	
5	0.78	0.69			0.00	0.09	0.22	
6	0.93	0.11				0.83	0.06	
7	1.00	1.04			–0.05	–0.05	0.00	
8	0.45	0.24				0.21	0.55	
9	0.86	1.05			–0.40	–0.19	0.14	
10	0.72	0.66			0.00	0.06	0.29	
11	1.04	1.27			0.23	–0.23	–0.04	
12	0.53	0.78			–0.04	–0.24	0.47	
13	0.5	0.64				–0.14	0.50	
14	0.57	0.36			0.22	0.21	0.43	
15	0.70	0.39			–0.06	0.31	0.30	
16	0.56	0.62			0.04	–0.06	0.45	
17	0.69	0.70			0.08	–0.01	0.31	
18	0.47	0.53	0.45	0.40		–0.06	0.53	–0.07
19	0.88	0.66	0.77	0.98		0.21	0.12	0.10
20	1.13	0.48	0.83	1.48		0.65	–0.13	0.35
21	0.66	0.39	0.43	0.70		0.26	0.34	0.04
22	0.56	1.60	1.19	0.15		–1.04	0.44	–0.41
23	1.17	0.89	0.61	0.88		0.28	–0.17	–0.28
24	0.72	0.52	1.26	1.46		0.20	0.28	0.74
25	0.74	0.30	0.79	1.22		0.43	0.26	0.48

three columns. In contrast to other studies, we present and analyze all measurements, not only average values. Otherwise it is impossible to find systematic errors of measurements and features of the Fontan circulation.

Hydrodynamic mathematical models guarantee mass conservation. For local 3D blood flow models total net forward blood volume in vena cava should be equal to the total net forward blood volume in pulmonary arteries $V_{VC} = V_{IVC} + V_{SVC} = V_{PA} = V_{RPA} + V_{LPA}$ in the absence of blood outflows in the TCPC domain. Both total net forward blood volumes should be equal to the net forward blood volume in aorta and pulmonary veins $V_{Aorta} = V_{VC} = V_{PA} = V_{PV}$. These equalities do not hold for real data. We recall that relative errors in measurements may be as high as 22.5% of typical VENC [28]. If VENC for 4D flow MRI is set to 80–150 $\mathrm{cm\,s^{-1}}$, the absolute error of blood velocity measurements may reach 18–33 $\mathrm{cm\,s^{-1}}$ that corresponds to the net forward volume 20–30 ml. For most patients values of possible errors are comparable to net forward blood volume in vena cava and pulmonary arteries, *cf.* Table 2.

In Table 3, we present the data in relation to the net blood volume in aorta. Since the blood velocity in aorta is comparable to VENC, the relative error of measurement may achieve $\frac{V_{error}}{V_{Ao}} \sim 0.225$. In Cols. 2–4 we analyze blood distribution for real data. We present net forward blood volume in vena cava, pulmonary arteries and pulmonary veins in relation to the net blood volume in aorta: $\frac{V_{VC}}{V_{Ao}}$, $\frac{V_{PA}}{V_{Ao}}$, $\frac{V_{PV}}{V_{Ao}}$. Only for 9 patients out of 25 the total net forward blood volume in vena cava deviates from that in aorta for less than 22%; only for 7 patients out of 25 the total net forward blood volume in pulmonary arteries deviates from that in aorta for less than 22%, only for 3 patients out of 8 the total net forward blood volume in pulmonary veins deviates from that in

aorta for less than 22%. Therefore, collateral and/or fenestration blood flow occurs in the Fontan circulation for most patients.

Also we calculated the total venous return by common formula $V_{VR} = V_{VC} + V_{PV} - V_{PA}$ [11]. This formula takes into account the fenestration flow. Venous return should be equal to the aortic blood volume leaving the heart and the relative blood volume of the venous return V_{VR}/V_{Ao} should be equal to 1. The data is presented in the Col. 5 of the Table 3. Only for 3 patients of 8 the value is close to 1: the deviation is less than 0.22. This implies that the error in flow estimation is significant and systematic.

Conduit is a tube with a constant area of cross section along it. Previously [12] we found that 4D flow data shows flow pulsations in the conduit and areas of conduit cross-sections are underestimated significantly compared to the same measurements due to cine MRI. The reason was presence of domains with slow blood flow which generate assessment errors. IVC passes into the conduit, and blood flows are expected to be equal in these two vessels, in the absence of fenestration.

We estimated the volume of blood passing through the fenestration in two different ways. Firstly, it was calculated as a difference of blood volume before and after fenestration $V_F = V_{IVC} - V_{cond}$. The relative value $V_F^R = V_F/V_{Ao}$ is presented in the 6th column of Table 3. Only for patient 11 it exceeds 0.22 and may be attributable to presence of fenestration. For patient 9 $V_F = -0.4$: its module exceeds 0.22, but the sign is negative. This may be attributable to blood reflux in the conduit or to measurement errors. Secondly, the volume of blood passing through the fenestration was calculated by the conventional formula [11]: $V_F = V_{VC} - V_{PA}$. The relative value V_F^R is presented in the 7th column of Table 3. For 9 patients out of 25 its module exceeds 0.22, for 6 of them the sign is positive and may be attributable to presence of fenestration (patients 6, 15, 20, 21, 23, 25). Values of V_F^R calculated by different formulas are consistent for 10 patients of 13 patients having both data in 6 and 7 columns. For patient 14 both values V_F^R indicate the flow through fenestration. Remarkably, there is no patients for which both values confirm the blood flow through fenestration. Visual confirmation of flow through the fenestration is difficult or impossible.

Another feature of the Fontan circulation is developed collateral blood flow. The blood volume through systemic collaterals is $V_{SC} = V_{Ao} - (V_{SVC} + V_{IVC})$ [11]. The corresponding relative volume $V_{SC}^R = V_{SC}/V_{Ao}$ ranges from 0 to 0.55 for Fontan patients (the 8th column of Tab. 3), it exceeds 0.22 for 16 of them, exceeds 0.3 for 12 patients, exceeds 0.4 for 9 patients, exceeds 0.5 for 2 patients.

For 8 patients we have additional data for the net forward blood volume in pulmonary veins, so we can calculate the blood volume which goes through pulmonary collaterals: $V_{PC} = (V_{RPV} - V_{RPA}) + (Q_{LPV} - Q_{LPA})$ [11]. The relative volume $V_{PC}^R = V_{PC}/V_{Ao}$ is up to 0.74 (the 9th column of Tab. 3). Systemic and pulmonary collateral blood volumes should be equal. However, only for 3 patients of 8 the values of V_{SC}^R and V_{PC}^R are consistent (the difference is 0.22 or less).

4D flow MRI data of patients after the Glen procedure may be used for predictive modelling of the Fontan procedure. Analysis of such data gave the same results: we found inconsistency of mass conservation law and appearance of collateral blood flow. This data set was poor comparing to the 4D flow MRI data set of patients with Fontan circulation, discussed in this section, and is not presented here.

3.3. Comparison of 4D flow and 2D phase contrast MRI data

In order to verify data from Table 2 we compare it with the results of 2D phase contrast tomography. The 2D phase contrast MRI is the golden standard of flow rate assessment. This data is available for patients 18–25 and Tables 4 and 5 are direct analogs of Tables 2 and 3, with the same flow characteristics.

For patients 18,20,22,24, the net forward flow volume in aorta measured by 2D phase contrast MRI is significantly higher than that measured by 4D flow MRI scanning. The net forward flow volume in IVC measured by 2D Phase contrast MRI is also significantly higher for 6 patients of 8. Measurements of the net forward flow volume in SVC, RPA, LPA are different in these two MRI modes. Blood flow distribution between RPA and LPA calculated by 2D phase contrast MRI and 4D flow MRI are similar only for patient 21, for other seven patients the distributions are different. Significant deviations are attributable most likely to different VENC parameters for two methods: it is higher for aorta and lower for veins in 2D phase contrast method.

TABLE 4. 2D phase contrast MRI measurements of net forward volume [ml] for Fontan patients in Aorta (Ao) and Vena Cava (VC), Pulmonary arteries (PA): Inferior and Superior Vena Cava (IVC and SVC), conduit (cond), Right and Left pulmonary arteries (RPA and LPA).

No	Ao	IVC	SVC	cond	RPA	LPA	VC	PA
18	46,3	25.1	6.7	25.4	5.5	5.6	31.8	11.1
19	42	29.7	17.9	30.6	7	10	47.6	17
20	53.5	15.9	13.4	14.6	2.3	3.3	29.3	5.6
21	66.5	30.8	14.5	27.8	16	3.6	45.3	19.6
22	63.2	43.7	16.2	43.1	14	14.8	59.9	28.8
23	17.2	28.6	14.1	29.9	1.7	13.2	42.7	14.9
24	38.6	25.7	10.5	27	2.7	10.5	36.2	13.2
25	23	24.5	2.3	22.6	3.3	8	26.8	11.3

TABLE 5. Net forward blood volume in Vena Cava and Pulmonary arteries (VC and PA) – Cols. 2–3; fenestration – Cols. 4–5; collaterals – Col. 6 relative to the net forward blood volume in Aorta (Ao) for Fontan patients calculated based on 2D phase contrast MRI measurements.

1	2	3	4	5	6
No	$\frac{V_{VC}}{V_{Ao}}$	$\frac{V_{PA}}{V_{Ao}}$	$\frac{V_{IVC}-V_{cond}}{V_{Ao}}$	$\frac{V_{VC}-V_{PA}}{V_{Ao}}$	$\frac{V_{SC}}{V_{Ao}}$
18	0.68	0.24	–0.01	0.45	0.31
19	1.14	0.41	–0.02	0.73	–0.13
20	0.55	0.10	0.02	0.44	0.45
21	0.68	0.29	0.05	0.39	0.32
22	0.95	0.45	0.01	0.49	0.05
23	2.48	0.87	–0.08	1.62	–1.48
24	0.94	0.34	–0.03	0.60	0.06
25	1.17	0.49	0.08	0.67	–0.17

The volume of blood flow passing through fenestration $V_{IVC} - V_{cond}$ (the 4th column of Tab. 5) does not exceed 8% of the aortic blood volume, *i.e.* the blood flow through fenestration is absent or negligible. On the other hand, the conventional formula for $V_{VC} - V_{PA}$ indicates to significant flow rates through fenestration (the 5th column of Tab. 5). These values in the 4th and the 5th columns are inconsistent with each other and with the same data extracted from 4D flow measurements. Collateral blood flow is confirmed by both methods only for patients 18 and 21.

To summarize, the blood flow volumes in aorta, systemic veins, and pulmonary arteries measured by the 2D phase contrast and 4D flow MRI methods are different and hence all calculated indices are different either. The differences are attributable to a rough choice of parameter VENC (80–100 $\mathrm{cm\,s^{-1}}$ for all vessels [10]) that generates larger errors in 4D flow MRI compared to the 2D phase contrast MRI measurement where VENC depends on the vessel: 50–80 $\mathrm{cm\,s^{-1}}$ (usually 60 $\mathrm{cm\,s^{-1}}$) for systemic veins and pulmonary veins and arteries and 150–200 $\mathrm{cm\,s^{-1}}$ (usually 150 $\mathrm{cm\,s^{-1}}$) for aorta [32]. It is recommended that the VENC be set to approximately 25% above the expected maximum velocity so as to optimize the dynamic range [33].

The errors of both methods are contributed by noise, low spatial resolution, segmentation in post-processing, vortex flow appearance [26, 28]. The 2D phase contrast data acquisition is also affected by respiration phases (respiration is averaged and not so notable for lengthy 4D flow mapping) [30]. Moreover, since the highest measured velocity may be at some distance from the scanning plane, it is difficult to determine accurately the peak velocity. According to the literature, the ability to assess blood flow in all large vessels simultaneously and in any orientation makes the 4D flow mapping the most appealing estimation of the Fontan blood circulation despite possible methodological costs [28].

Both overestimation and underestimation of some hemodynamic parameters measured by 4D flow MR method were reported in the literature [34–38]. According to some studies, hemodynamic 4D flow MR measurements corresponds to the same data provided by the 2D phase-contrast MR imaging in large arteries [39]. This information should be verified in future.

4. Illustration of mathematical model initialization with discussed patient-specific data

In this section we illustrate initialization of patient-specific hemodynamic models for Fontan patients. In local 3D models the domain of interest Ω consists of conduit, SVC, IVC, LPA and RPA and should be segmented from CT (preferably) or MRI data. The blood is considered to be newtonian viscous incompressible fluid (with viscosity ν and density ρ), the boundary of the 3D domain Ω includes rigid (in a simple case) walls Γ_0 and inlets/outlets $\Gamma_{in/out}$. The blood flow is described by the 3D Navier–Stokes equations

$$\rho\left(\frac{\partial \mathbf{u}}{\partial t} + (\mathbf{u}\cdot\nabla)\,\mathbf{u}\right) - \nu\Delta\mathbf{u} + \nabla p = \mathbf{f} \quad \text{in } \Omega, \qquad \operatorname{div}\mathbf{u} = 0 \tag{4.1}$$

where p is the pressure, $\mathbf{u}$ is the velocity vector field, $\mathbf{n}$ is the outward normal vector, $\mathbf{f}$ is an external force. No-slip and no-penetration boundary conditions are assumed on rigid walls Γ_0. Inhomogeneous Dirichlet ($\mathbf{u} = \mathbf{g}$ with given blood velocity distribution $\mathbf{g}$) or Neumann ($\nu\frac{\partial \mathbf{u}}{\partial \mathbf{n}} - p\mathbf{n} = \gamma\mathbf{n}$ with known average pressure γ on the cross section) boundary condition should be posed on each inlet or outlet $\Gamma_{in/out}$. In addition, $\mathbf{u} = \mathbf{u}_0$ ($\operatorname{div}\mathbf{u}_0 = 0$) for $t = 0$ is a given initial condition. Numerical simulations require setting a boundary condition on each boundary $\Gamma_{in/out}$ based on clinical data. The solution of (4.1) is very sensitive to the boundary conditions. MRI measurements do not guarantee even the mass conservation in the domain Ω. Possible pressure measurements are also rather inaccurate. Therefore, personalization of the 3D flow model (4.1) is complicated.

Coupling the local 3D blood flow model with a 1D model of circulation avoids the issue of setting boundary conditions for the following reasons. The 1D model is derived from the Navier–Stokes equations by their averaging over the vascular cross section [13, 40]. Each vessel is represented by a long enough collapsible elastic tube. The continuities of certain flow characteristics are required at the interface of 1D and 3D models, for example, flow rate and normal stress. The problem of setting boundary conditions is transferred from TCPC inlets and outlets to regions where the flow rate can be measured more reliably, *e.g.* MR 4D flow examination in aorta or Doppler data in accessible vessels where flow rate, blood velocity or pressure may be prescribed. This problem disappears completely if the 1D-3D model is a closed circulation model fitted to the patient. If the clinical data used for model initialization does not ensure mass conservation, collateral flows or flow through fenestration may be included in the 1D model.

The size of the 1D component may be varied depending on available clinical data. The two-scale 1D-3D model can be personalized based on (mandatory for the patient) ultrasound and anthropometric measurements. Some methods of personalization are presented in [13].

An example of personalized 1D-3D blood flow model for a patient with Fontan circulation (*cf.* No. 17 in Tab. 2) is presented in [12].

5. Conclusion

Optimization of the Fontan procedure demands patient-specific preoperative blood flow models. Construction of the computational domain and setting boundary conditions are the most important steps of patient-specific simulations. CT is a routine examination before the Fontan procedure. CT provides images of high quality allowing to segment accurately the domain of interest. MRI is performed less frequently. MRI data may be used for segmentation as well, but the image resolution is lower. Higher resolution is possible in a smaller domain of interest because of examination duration. The quality of segmentation depends on the quality of medical

images, in particular, on the contrast of organs (arteries, veins, ventricles, atria, *etc.*). 3D domain segmented from MRI data is much smaller than the same domain for the same patient segmented from CT data.

Local hemodynamic models require prescribing inflow boundary conditions at levels of IVC and SVC. Postoperative SVC and IVC flow rates are unknown. Preoperative flow rates may be estimated by 2D phase-contrast and 4D flow MRI. We analyzed such data for patients with the Fontan circulation. Comparison of 2D and 4D flow data in TCPC shows inconsistency of most measurements. The error of measurement is high and its value approaches blood velocity in veins. Among possible reasons are unsuitable (high) parameter VENC, slow and/or complex blood flow, reflux, high noise-to-signal ratio.

Even the net forward blood volume in aorta estimated by 2D phase contrast MRI exceeds that estimated by 4D flow MRI. A possible reason may be higher VENC value for the 2D phase contrast measurement. If blood velocity does not exceed VENC, the results of 2D phase contrast and 4D flow MRIs are comparable.

In view of the above difficulties, global blood flow models seem to be more applicable for Fontan procedure prediction. They may be personalized using more reliable MRI-estimation of the flow rate in aorta and Doppler data in accessible vessels [13, 41, 42]. Global models benefit from accounting changes of inflow boundary conditions after the Fontan procedure and may consider collateral and fenestration blood flows typical for the Fontan circulation. Collateral blood flow may be estimated by 2D phase contrast or 4D flow MRI measurements although the methodology of such measurement is to be refined.

Acknowledgements

The study was performed at Marchuk Institute of Numerical Mathematics RAS and supported by the Russian Science Foundation (project 21-71-30023). The authors are grateful to Ksenia Slepova for the assistance in image processing.

References

[1] A. Corno, M. Owen, A. Cangiani, E. Hall and A. Rona, Physiological Fontan procedure. *Front. Pediatr.* **7** (2019).

[2] M. Schafstedde, P. Yevtushenko, S. Nordmeyer, *et al.*, Virtual treatment planning in three patients with univentricular physiology using computational fluid dynamics-pitfalls and strategies. *Front. Cardiovasc. Med.* **9** (2022).

[3] K. Marshall, Y. D'Udekem, G. Sholler, *et al.*, Health-related quality of life in children, adolescents, and adults with a Fontan circulation: a meta-analysis. *J. Am. Heart Assoc.* **9** (2020) e014172.

[4] T. Fredenburg, T. Johnson and M. Cohen, The Fontan procedure: anatomy, complications, and manifestations of failure. *RadioGraphics* **31** (2011) 453–463.

[5] I. Schwartz, C. McCracken, Ch. Petit and R. Sachdeva, Late outcomes after the fontan procedure in patients with single ventricle: a meta-analysis. *Heart* **104** (2018) 1508–1514.

[6] P. Trusty, T. Slesnick, Z. Wei, *et al.*, Fontan surgical planning: previous accomplishments, current challenges, and future directions. *J. Cardiovasc. Trans. Res.* **11** (2018) 133–144.

[7] D. de Zelicourt and V. Kurtcuoglu, Patient-specific surgical planning, where do we stand? The example of the Fontan procedure. *Ann. Biomed. Eng.* **44** (2016) 174–186.

[8] W. Yang, F. Chan, V. Reddy, *et al.*, Flow simulations and validation for the first cohort of patients undergoing the Y-graft Fontan procedure. *J. Thorac. Cardiovasc. Surg.* **149** (2015) 247–255.

[9] A. Baretta, C. Corsini, W. Yang, *et al.*, Modelling of congenital hearts alliance (MOCHA) investigators. Virtual surgeries in patients with congenital heart disease: a multi-scale modelling test case. *Philos. Trans.* **369** (2011) 4316–4330.

[10] F. Raimondi, D. Martins, R. Coenen, *et al.*, Prevalence of venovenous shunting and high-output state quantified with 4D flow MRI in patients with Fontan circulation. *Radiology Cardiothorac. Imaging* **3** (2021) e210161.

[11] K. Whitehead, M. Harris, A. Glatz, *et al.*, Status of systemic to pulmonary arterial collateral flow after the Fontan procedure. *Am. J. Cardiol.* **115** (2015) 1739–1745.

[12] T. Dobroserdova, Yu. Vassilevski, S. Simakov, *et al.*, Two-scale haemodynamic modelling for patients with Fontan circulation. *Russ. J. Numer. Anal. Math. Model.* **36** (2021) 267–278.

[13] Yu. Vassilevski, M. Olshanskii, S. Simakov, *et al.*, Personalized Computational Hemodynamics. Models, Methods, and Applications for Vascular Surgery and Antitumor Therapy. Academic Press (2020).

[14] P. Hoskins, K. Martin and A. Thrush, Diagnostic Ultrasound: Physics and Equipment, 2nd edn. Cambridge: Cambridge University, 2010.

[15] P. Ciliberti, P. Ciancarella, P. Brun, *et al.*, Cardiac imaging in patients after Fontan palliation: which test and when? frontiers in pediatrics. *Front Pediatr.* **10** (2022).

[16] T. Leiner, J. Bogaert, M. Friedrich, *et al.*, SCMR position paper (2020) on clinical indications for cardiovascular magnetic resonance. *J. Cardiovasc. Magn. Reson.* **22** (2020).

[17] S. Moscatelli, N. Borrelli, J. Sabatino, *et al.*, Role of cardiovascular imaging in the follow-up of patients with Fontan. *Circulation* **9** (2022).

[18] P. Ciliberti, P. Ciancarella, P. Brun, *et al.*, Cardiac imaging in patients after Fontan palliation: which test and ehen? *Front. Pediatr.* **10** (2022).

[19] T. Leiner, J. Bogaert, M. Friedrich, *et al.*, SCMR position paper (2020) on clinical indications for cardiovascular magnetic Resonance. *J. Cardiovasc. Magn. Reson.* **22** (2020).

[20] W. Loughborough, M. Yeong and M. Hamilton, Computed tomography in congenital heart disease: how generic principles can be applied to create bespoke protocols in the Fontan circuit. *Quant. Imaging Med. Surg.* **7** (2017) 79–87.

[21] K. Pushparajah, Ph. Duong and S. Mathur, Cardiovascular MRI and CT in congenital heart disease. *Echo Res. Pract.* **6** (2019) R121–R138.

[22] T. Leiner, J. Bogaert, M. Friedrich, *et al.*, SCMR position paper (2020) on clinical indications for cardiovascular magnetic resonance. *J. Cardiovasc. Magn. Reson.* **22** (2020).

[23] P. Yushkevich, J. Piven, C. Heather, *et al.*, User-guided 3D active contour segmentation of anatomical structures: significantly improved efficiency and reliability. *Neuroimage* **31** (2006) 1116–1128.

[24] M. Terada, Y. Takehara, H. Isoda, *et al.*, Technical background for 4D flow MR imaging. *Magn. Reson. Med. Sci.* **21** (2022) 267–277.

[25] H. Isoda and A. Fukuyama, Quality control for 4D flow MR imaging. *Magn. Reson. Med. Sci.* **21** (2022) 278–292.

[26] H. Ha, Accuracy evaluation of blood flow distribution in the Fontan circulation: effects of resolution and velocity noise. *J. Visual* **22** (2019) 245–257.

[27] J. Geiger, F. Callaghan, B. Burkhardt, *et al.*, Additional value and new insights by four-dimensional flow magnetic resonance imaging in congenital heart disease: application in neonates and young children. *Pediatr. Radiol.* **51** (2021) 1503–1517.

[28] K. Jarvis, S. Schnell, A. Barker, *et al.*, Caval to pulmonary 3D flow distribution in patients with Fontan circulation and impact of potential 4D flow MRI error sources. *Magn. Reson. Med.* **81** (2019) 1205–1218.

[29] J. Garay, H. Mella, J. Sotelo, *et al.*, Assessment of 4D flow MRI's quality by verifying its Navier–Stokes compatibility. *Magn. Reson. Med.* **38** (2022).

[30] D. Rutkowski, G. Barton, Ch. Francois, *et al.*, Analysis of cavopulmonary and cardiac flow characteristics in Fontan patients: comparison with healthy volunteers. *J. Magn. Reson. Imaging* **49** (2019) 1786–1799.

[31] F. Puricelli, I. Voges, P. Gatehouse, *et al.*, Performance of cardiac MRI in pediatric and adult patients with Fontan circulation. *Radiol. Cardiothorac. Imaging* **4** (2022).

[32] Ph. Trusty, T. Slesnick, Zh. Wei, *et al.*, Fontan surgical planning: previous accomplishments,current challenges, and future directions. *J. Cardiovasc. Transl. Res.* **11** (2018) 133–144.

[33] S. Fratz, T. Chung, G. Greil, *et al.*, Guidelines and protocols for cardiovascular magnetic resonance in children and adults with congenital heart disease: SCMR expert consensus group on congenital heart disease. *J. Cardiovasc. Magn. Reson.* **15** (2013).

[34] A. Stalder, M. Russe, A. Frydrychowicz, *et al.*, Quantitative 2D and 3D phase contrast MRI: optimized analysis of blood flow and vessel wall parameters. *Magn Reson. Med.* **60** (2008) 1218–1231.

[35] L. Brix, S. Ringgaard, A. Rasmusson, *et al.*, Three dimensional three component whole heart cardiovascular magnetic resonance velocity mapping: comparison of flow measurements from 3D and 2D acquisitions. *J. Cardiovasc. Magn. Reson.* **11** (2009).

[36] M. Gabbour, S. Schnell, K. Jarvis, *et al.*, 4-D flow magnetic resonance imaging: blood flow quantification compared to 2-D phase-contrast magnetic resonance imaging and Doppler echocardiography. *Pediatr. Radiol.* **45** (2015) 804–813.

[37] K. Jarvis, M. Vonder, A. Barker, *et al.*, Hemodynamic evaluation in patients with transposition of the great arteries after the arterial switch operation: 4D flow and 2D phase contrast cardiovascular magnetic resonance compared with Doppler echocardiography. *J. Cardiovasc. Magn. Reson.* **18** (2016) 59.

[38] M. Sieren, C. Berlin, T. Oechtering, *et al.*, Comparison of 4D flow MRI to 2D flow MRI in the pulmonary arteries in healthy volunteers and patients with pulmonary hypertension. *PLoS One* **14** (2019).

[39] B. Burkhardt, Ch. Kellenberger, F. Callaghan, *et al.*, Flow evaluation software for four-dimensional flow MRI: a reliability and validation study. *Acad. Radiol.* **128** (2023) 1225–1235.

[40] A. Quarteroni and L. Formaggia, Mathematical modelling and numerical simulation of the cardiovascular system, in Computational Models for the Human Body. Vol. 12 of *Handbook of Numerical Analysis*. Elsevier (2004) 3–127.

[41] T. Gamilov, Yu. Ivanov, P. Kopylov, *et al.*, Patient specific haemodynamic modeling after occlusion treatment in leg. *Math. Model. Nat. Phenom.* **9** (2014) 85–97.

[42] D. Burenchev, F. Kopylov, A. Bykova, *et al.*, Mathematical modelling of circulation in extracranial brachocephalic arteries at pre-operation stage in carotid endarterectomy. *Russ. J. Cardiol.* **4** (2017) 88–92.